REPORTS

APPLIED ORIGAMI

Origami of thick panels

Yan Chen,[1] Rui Peng,[1] Zhong You[2]*

Origami patterns, including the rigid origami patterns in which flat inflexible sheets are joined by creases, are primarily created for zero-thickness sheets. In order to apply them to fold structures such as roofs, solar panels, and space mirrors, for which thickness cannot be disregarded, various methods have been suggested. However, they generally involve adding materials to or offsetting panels away from the idealized sheet without altering the kinematic model used to simulate folding. We develop a comprehensive kinematic synthesis for rigid origami of thick panels that differs from the existing kinematic model but is capable of reproducing motions identical to that of zero-thickness origami. The approach, proven to be effective for typical origami, can be readily applied to fold real engineering structures.

O rigami is the art of folding essentially two-dimensional materials such as paper into three-dimensional objects. It has recently gained popularity among scientists and engineers because the technique can be used to create shape-changing structures. Rigid origami is a subset of origami that considers rigid objects connected by hinges. This type of origami has probably the greatest application potential in engineering structures (1, 2)—ranging from solar panels (3), space mirrors, and aircraft wings, to robots (4)—because most materials used in these applications are relatively rigid. To date, all kinematic modeling of rigid origami treats the paper as having zero thickness. At each vertex where creases, or fold lines, meet, the origami is considered as a spherical linkage, where creases act as revolute joints (R) and the paper bounded by the creases act as links. A rigid origami pattern is therefore a combination of many such linkages. For panels of nonzero thickness, various techniques have been suggested to use the same kinematic model, which include adding tapered materials to the plane of zero-thickness (5) or offsetting panels away from the planes defined by the adjacent creases (6). The tapered material technique has been used to fold a thick panel based on the Miura-ori, whereas the offset one has been used for folding a square-twist origami pattern. However, these methods often result in surfaces that are either not entirely flat or with voids to allow folding. Two exceptions to this are the technique introduced by Hoberman to fold the symmetric Miura-ori (7), and the technique by De Temmerman for the diamond origami pattern (8). Not all of the fold lines meet at a point in either of these methods, and thus, the vertices no longer exist. This indicates that their folding cannot be simply treated as the motion

of spherical linkage assemblies. This has led us to question what a rigorous equivalent kinematic model of this type of origami should be, and whether the model can be generalized and applied so as to create origami for thick materials.

Rigid origami patterns, designed universally for a zero-thickness sheet, are made from creases intersecting at vertices. However, these patterns cannot be directly applied to a panel of nonzero thickness, given that all of the fold lines cannot be placed on the same face of the panel because the subpanels would collide during folding. For this reason, some fold lines must be placed on the top face whereas others must be placed on the bottom face of a panel, forming an assembly in which the fold lines are neither concurrent nor intersecting at a vertex. As a result, the kinematic model of the spherical linkage around each vertex used for a zero-thickness sheet has now been replaced by a loop of rigid bodies (panels) connected by a set of revolute joints (fold lines) that are placed a distance apart because of the thickness. Its foldability depends on two conditions: (i) Each loop of connected rigid bodies must be a mechanical linkage, and (ii) the assembly of these linkages retains mobility so that it can be folded.

Most practically used patterns—such as the Miura-ori, square-twist, diamond, and waterbomb patterns—have four, five, or six creases intersecting at a vertex, and thus, the corresponding closed kinematic chains for thick panels, when foldable, are spatial 4R, 5R, and 6R linkages. These linkages belong to a specific family of spatial linkages often referred to as the overconstrained linkages because the Kutzbach criterion yields a mobility value of less than one (9). The existence of mobility is due to specific geometries that the linkages possess. In this work, we first found the kinematically equivalent spatial linkages to the single-vertex origami patterns made from four, five, and six creases, respectively, and then extended this to multiple vertex patterns by ensuring that the motion of the assembly of these linkages matches that of the zero-thickness pattern. Using this approach, origami patterns

can still be designed based on a zero-thickness rigid sheet, and these patterns can consequently be synthesized for a thick rigid panel. We assume that thick panels are rigid with nonzero thickness and that fold lines, equivalent to creases in zero-thickness paper and revolute joints in linkages, can only be placed on the faces of a thick panel, and no fold lines along the depth of the panels are permitted.

A partially folded single-vertex four-crease origami pattern of a zero-thickness rigid sheet is shown in Fig. 1A. This pattern is the basic element in many well-known origami forms, such as the Miura-ori and the square-twist pattern. Four creases divide the sheet into four portions, with sector angles α_{12}, α_{23}, α_{34}, and α_{41}, respectively, and the sum of these angles equals 2π. To be flat foldable—the folded origami can be pressed flat eventually—$\alpha_{12} + \alpha_{34} = \alpha_{23} + \alpha_{41} = \pi$ must be satisfied (10).

The kinematic motion of this origami can be modeled as a spherical 4R linkage. It has a single degree of freedom, and the relationship among four dihedral angles φ_1, φ_2, φ_3, and φ_4 can be obtained analytically (11)

$$\frac{\tan\frac{\varphi_2}{2}}{\tan\frac{\varphi_1}{2}} = -\frac{\sin\frac{\alpha_{12} - \alpha_{23}}{2}}{\sin\frac{\alpha_{12} + \alpha_{23}}{2}}, \varphi_1 = \varphi_3 \text{ and } \varphi_2 = \varphi_4 \quad (1)$$

Now consider its thick-panel counterpart (Fig. 1B), in which the panel is partitioned by the same set of sector angles into four subpanels. Place one fold line on the top face of subpanels, three on bottom faces. a_{12}, a_{23}, a_{34}, and a_{41} are distances between adjacent fold lines, respectively, which effectively represent the thicknesses of the subpanels.

Kinematically, this assembly is no longer a spherical linkage. It must be a spatial 4R linkage if it is capable of motion. The only spatial 4R linkage is the Bennett linkage, a century-old mechanism in which the axes of revolute joints neither meet nor are parallel (12). The existence of mobility is due to the special geometry conditions (13), which are

$$\alpha_{12} + \alpha_{34} = \alpha_{23} + \alpha_{41} = \pi \quad (2)$$

$$a_{12} = a_{34}, a_{23} = a_{41} \quad (3)$$

and

$$\frac{a_{12}}{a_{23}} = \frac{\sin\alpha_{12}}{\sin\alpha_{23}} \quad (4)$$

Equation 2 matches the flat foldable condition for a zero-thickness sheet, whereas Eqs. 3 and 4 are conditions governing the placement of fold lines. The Bennett linkage has a single degree of freedom. We can prove that the relationships among the dihedral angles are identical to those in Eq. 1, except that φ_1, φ_2, φ_3, and φ_4 are replaced by φ_1^{Be}, φ_2^{Be}, φ_3^{Be}, and φ_4^{Be}, respectively. Its motion is therefore identical to that of the spherical 4R linkage throughout the entire folding process (fig. S4). The spherical 4R linkage and this Bennett linkage are kinematically equivalent as a result. The folding process of a zero-thickness rigid origami and its thick-panel counterpart is

[1]School of Mechanical Engineering, Tianjin University, 92 Weijin Road, Nankai District, Tianjin 300072, China. [2]Department of Engineering Science, University of Oxford, Parks Road, Oxford OX1 3PJ, UK.
*Corresponding author. E-mail: zhong.you@eng.ox.ac.uk
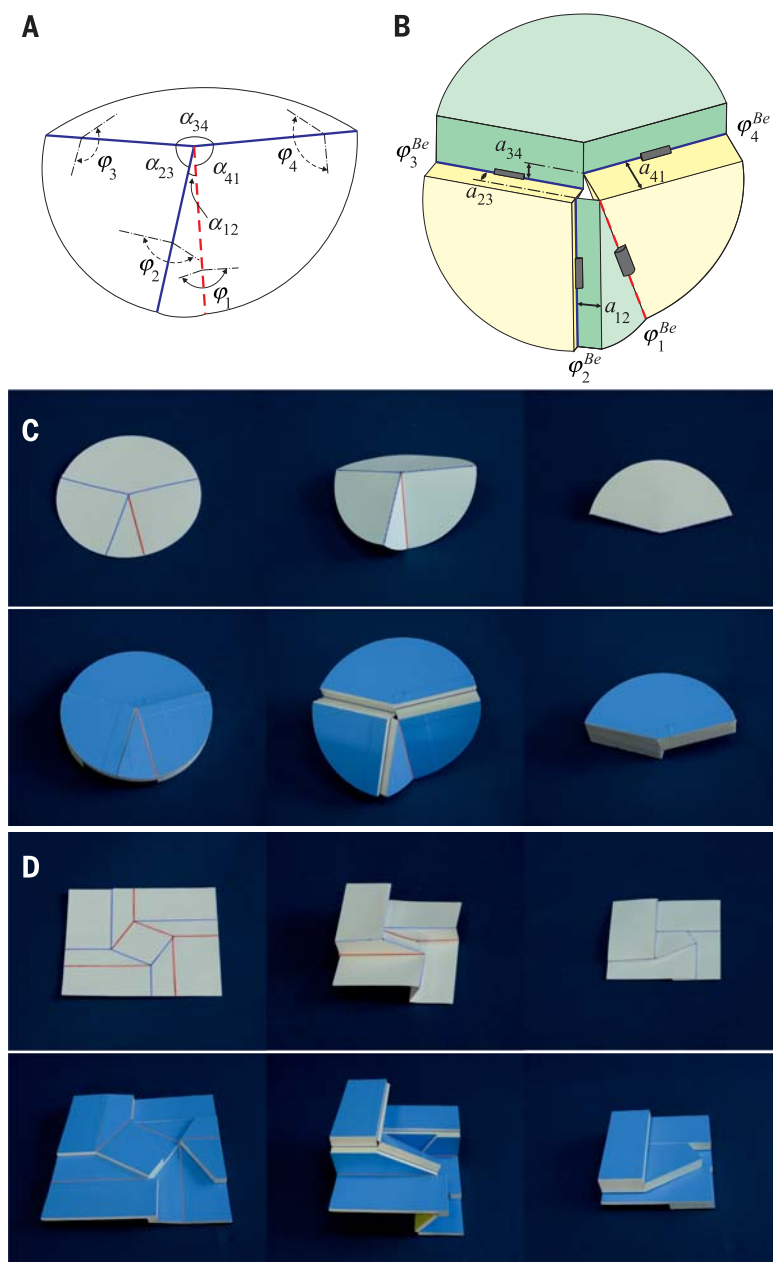
Fig. 1. Four-crease single- and multiple-vertex origami. (**A**) A partially folded single-vertex four-crease rigid origami for a zero-thickness sheet. Blue solid and red dash lines represent mountain and valley creases, respectively. αs and φs are sector and dihedral angles, respectively. (**B**) The thick-panel counterpart with the sector angles identical to those in (A), but the fold lines no longer meet at a point (vertex). as are distances between adjacent fold lines, and φ^{Be}s are dihedral angles. (**C**) Folding sequence of a model made of zero-thickness sheet and its thick-panel counterpart. The sector angles for both models are $\pi/6$, $\pi/2$, $5\pi/6$, and $\pi/2$. (**D**) Folding sequence of a zero-thickness square-twist origami and its thick-panel counterpart based on the Bennett linkage. The pattern consists of four identical four-crease vertices arranged in rotational symmetry. The sector angles for each vertex are the same as those for the single-vertex model in (C).

demonstrated in Fig. 1C and movie S1. Both have four fold lines, with the same sector angles.

The four-crease thick-panel origami can be readily applied to find the thick-panel equivalence of multiple-vertex rigid origami. For example, the square-twist pattern with rotational symmetry: First, the Bennett linkage can be applied to each vertex of the pattern, preserving the sector angle of each subpanel. We then merge the fold lines that are shared by two adjacent Bennett linkages. This is possible because there is rotational symmetry in the square-twist pattern, leading to the exact same amount of rotation for the combined fold lines. The folding process of a zero-thickness rigid panel

and its thick counterpart by using the square-twist pattern are shown in Fig. 1D, fig. S4, and movie S1.

Similarly, we can also create a folding scheme of a thick panel using the Miura-ori, as done by Hoberman (*7*). However, Hoberman only reported the symmetrical case in which $\alpha_{12} = \alpha_{23}$ and $\alpha_{34} = \alpha_{41}$, which is a special case of Eq. 2.

The Bennett linkage requires sector angles to satisfy Eq. 2 that equates to the condition for flat foldability. Because the Bennett linkage is the only known spatial $4R$ linkage, it can be concluded that for the four-crease rigid origami, only flat foldable patterns can have thick-panel equivalents.

The method for devising folding of four-crease patterns can be extended to the single-vertex five-crease rigid origami case. Many single-vertex five-crease origami patterns for a zero-thickness sheet exist, and here, we consider a particular one that has been used to make boxes (Fig. 2A). In this pattern, the creases divide the sheet into five pieces, with sector angles αs in which $\alpha_{51} = \alpha_{12}$, $\alpha_{23} = \alpha_{45} = \frac{\pi}{2}$, and $\alpha_{34} = \pi - 2\alpha_{12}$. It can be modeled as a spherical $5R$ linkage. In general, this linkage has two degrees of freedom, but we restrict its motion by preserving symmetry—that is, during folding, by letting the dihedral angles satisfy

$$\varphi_5 = \varphi_2 \text{ and } \varphi_4 = \varphi_3 \qquad (5)$$

We then consider its nonzero thickness counterpart (Fig. 2B), in which the thick panel is apportioned by exactly the same set of sector angles. The fold lines are then placed either on top or bottom of the panel surfaces, and the distances between a pair of neighboring fold lines are as. It has become a spatial $5R$ linkage.

There are a number of $5R$ overconstrained linkages. The arrangement of the sector angles makes it possible to be a Myard linkage (*14*) because it has the same angle conditions as those for this particular linkage. In addition, the Myard linkage requires

$$a_{12} = a_{51}, a_{23} = a_{45}, \text{ and } a_{34} = 0 \qquad (6)$$

and

$$\frac{a_{12}}{a_{23}} = \frac{\sin\alpha_{12}}{\sin\alpha_{23}} \qquad (7)$$

The thick-panel assembly will have one degree of freedom if the arrangement of fold lines satisfies Eqs. 6 and 7 because it is now a Myard linkage. Furthermore, the proof in the supplementary text shows that the motion of this linkage is identical to that of the spherical $5R$ linkage when Eq. 5 is imposed. This folding scheme has been used to fold a box (Fig. 2C and movie S1).

The Myard linkage has only one degree of freedom, whereas a spherical $5R$ linkage commonly has two. It is possible to find a kinematic match only if one of the degrees of freedom of the latter is frozen, which is achieved in the above example by imposing symmetry. The same strategy is used for the six-crease example discussed next.

One of the typical six-crease origami patterns is the diamond pattern. The zero-thickness pattern (Fig. 3A) has sector angles $\alpha_{12} = \alpha_{34} = \alpha_{45} = \alpha_{61}$ and $\alpha_{23} = \alpha_{56} = \pi - 2\alpha_{12}$. This spherical linkage has three degrees of freedom in general. However, if

**Fig. 2. Five-crease single- and multiple-vertex origami.** (**A**) A single-vertex five-crease rigid origami pattern for a zero-thickness sheet. (**B**) The thick-panel counterpart with sector angles identical to those in (A), but the fold lines no longer meet at a point (vertex). (**C**) Folding sequence of a zero-thickness rigid origami with five-crease vertices and its thick-panel counterpart based on the Myard linkage. The pattern has six five-crease vertices arranged in rotational symmetry. The sector angles at each vertex are $\pi/6$, $\pi/2$, $2\pi/3$, $\pi/2$, and $\pi/6$.
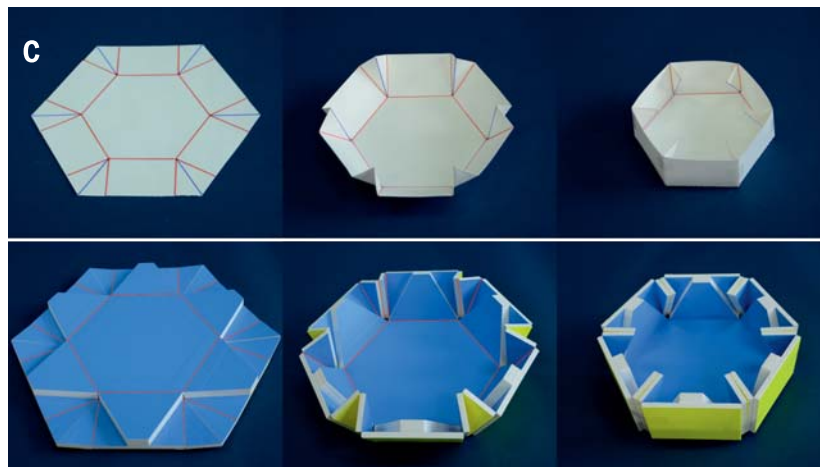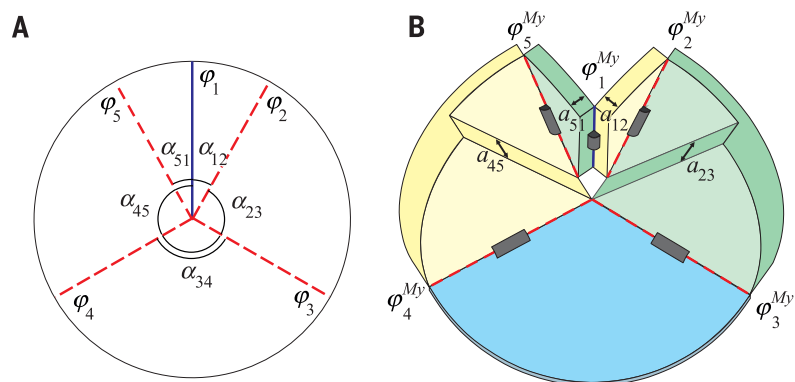

Fig. 3. The diamond origami pattern. (**A**) A single-vertex six-crease diamond pattern for a zero-thickness sheet. (**B**) The thick-panel counterpart with sector angles identical to those in (A), but the fold lines no longer meet at a point (vertex). (**C**) Folding sequence of a zero-thickness origami model of the diamond pattern and its thick-panel counterpart based on the plane-symmetric Bricard linkage. All the vertices are identical. The sector angles around each vertex are $\pi/6$, $2\pi/3$, $\pi/6$, $\pi/6$, $2\pi/3$, and $\pi/6$.
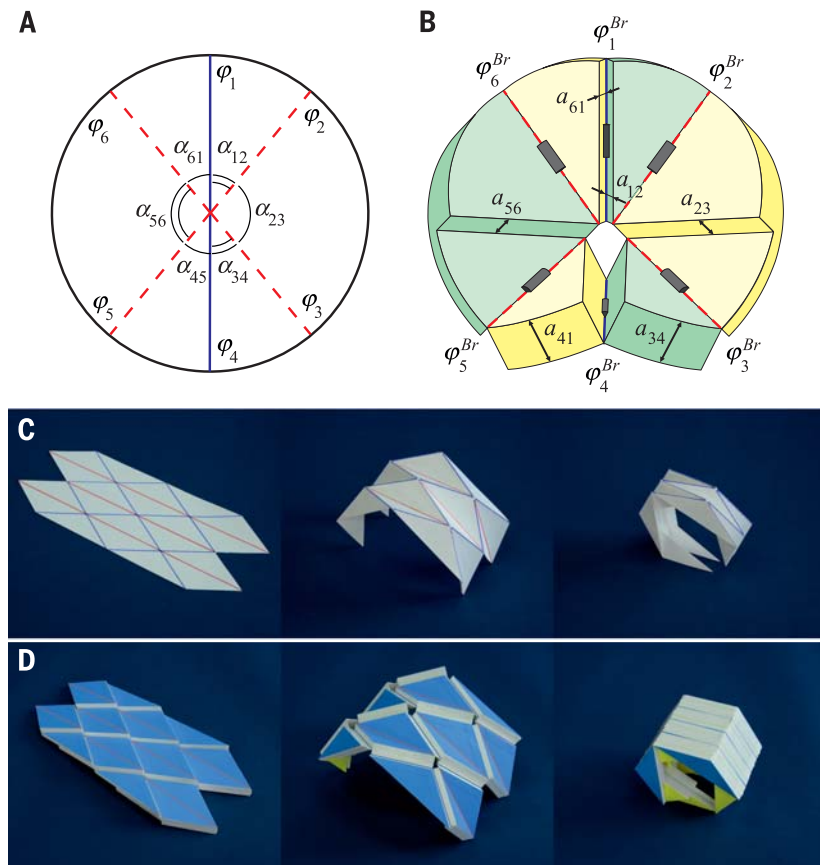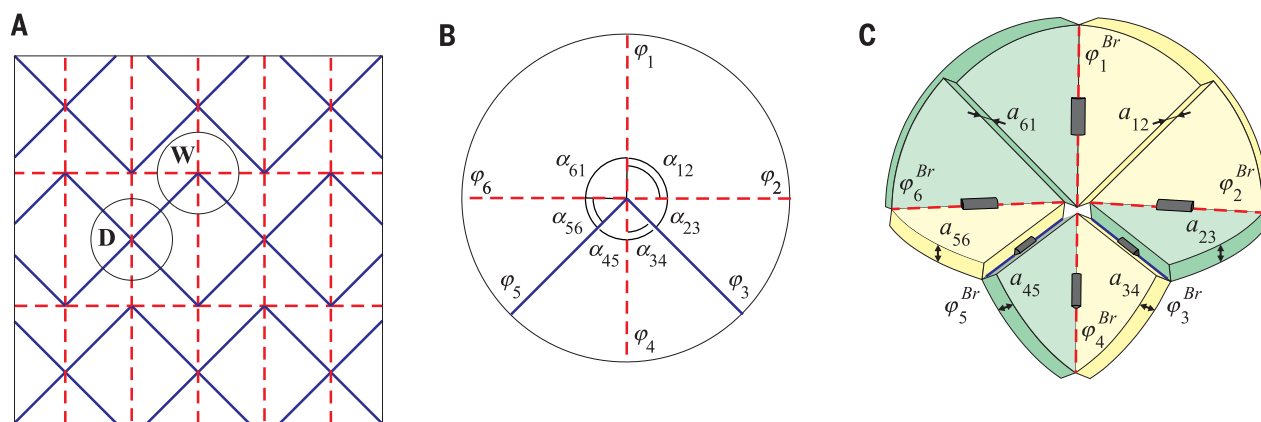
Fig. 4. Origami using the waterbomb pattern for zero- and nonzero-thickness panels and thick-panel origami of a pattern with a mixture of vertices with four and six creases. (**A**) The traditional waterbomb pattern for zero-thickness sheet. Two types of vertices are marked as **D** and **W**. (**B**) Origami pattern around vertex **W**. (**C**) Its thick-panel counterpart. (**D**) Folding sequence of the thick-panel waterbomb pattern. Around type **D** vertex, the sector angles are $\pi/4$, $\pi/2$, $\pi/4$, $\pi/4$, $\pi/2$, and $\pi/4$, whereas they are $\pi/2$, $\pi/4$, $\pi/4$, $\pi/4$, $\pi/4$, and $\pi/2$ around type **W** vertex. (**E**) Folding sequence of a thick-panel origami derived from an origami pattern with a mixture of both four- and six-crease vertices. It contains both the Bennett and Bricard linkages.
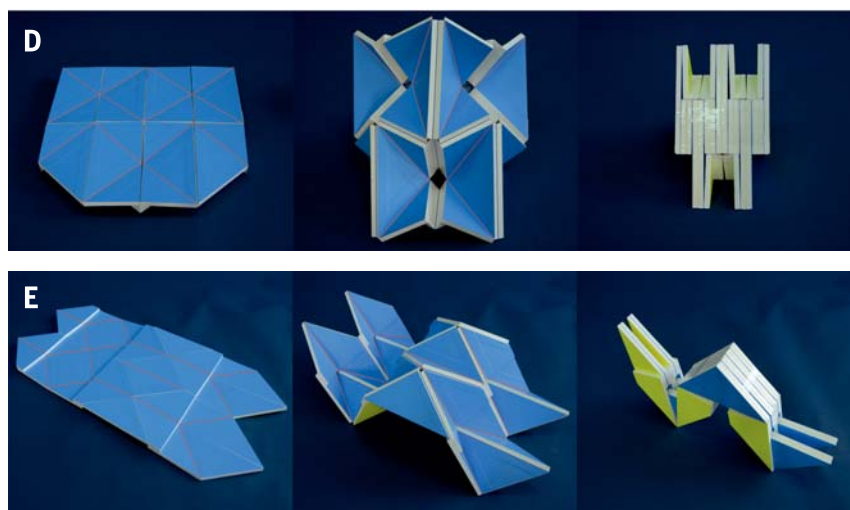
we confine its motions to the symmetric case by letting

$$\varphi_1 = \varphi_4 \text{ and } \varphi_2 = \varphi_3 = \varphi_5 = \varphi_6 \quad (8)$$

it reduces to a linkage with a single degree of freedom.

The corresponding thick-panel pattern is given in Fig. 3B, in which all sector angles are identical to those of the zero-thickness pattern. The distances between axes of fold lines are marked in the diagram.

The $6R$ assembly of Fig. 3B reassembles the plane-symmetric Bricard linkage (*15*) with line- and plane-symmetric behavior. The geometrical conditions of the Bricard linkage for the distances between neighboring axes of the rotational joints are

$$a_{12} = a_{61}, a_{23} = a_{56}, \text{and } a_{34} = a_{45} \quad (9)$$

In addition, to achieve compact folding, there must be

$$a_{12} + a_{23} = a_{34}, \quad (10)$$

which is obvious by considering the completely packaged configuration.

The kinematic motion of this Bricard linkage again matches that of the spherical $6R$ linkage of the zero-thickness model (fig. S8). This enables us to make a thick-panel origami arch using the

diamond pattern. The folding sequences of both zero- and nonzero-thickness models are shown in Fig. 3C and movie S1. This agrees with results reported by De Temmerman (*8*), but a complete mathematic proof is presented here.

Another typical six-crease origami pattern is the traditional waterbomb pattern (*16*), whose zero-thickness origami pattern is shown in Fig. 4A. Unlike the diamond pattern, there are two types of vertices, marked as **D** and **W**. **D** is a special case of the diamond pattern for which Eqs. 9 and 10 can be used to syntheses thick panel origami. **W**, specific to the waterbomb pattern, is enlarged in Fig. 4B, in which the sector angles are

$$\alpha_{12} = \alpha_{61} = \frac{\pi}{2} \text{ and}$$

$$\alpha_{23} = \alpha_{34} = \alpha_{45} = \alpha_{56} = \frac{\pi}{4} \quad (11)$$

For **W**, we can show that the corresponding Bricard linkage is a plane-symmetric one in which the thicknesses of subpanels must satisfy

$$a_{23} = a_{56}, a_{34} = a_{45} = \mu a_{23}, \text{and}$$

$$a_{12} = a_{61} = (1 + \mu)a_{23} \quad (12)$$

in order to achieve compact folding. μ is a constant. When $\mu = 1$, the motion of this Bricard

linkage is kinematically equivalent to that of the spherical linkage at **W**, as shown in Fig. 4C.

Considering the common folds appearing in both Bricard linkages as we did with the square-twist pattern described previously, the waterbomb pattern for the thick panel can be obtained. The folding sequence of nonzero thickness model is shown in Fig. 4D and movie S1.

If $\mu \neq 1$, the motion of the corresponding Bricard linkage differs from that of the spherical linkage at **W**, although both are flat foldable and can expand flat, which is demonstrated by the relationship between φ_1 (φ_1^{Br}) and φ_2 (φ_2^{Br}) in fig. S14. This indicates that the thick-panel origami can be devised by the mechanism theory alone without referring to its parent rigid origami pattern.

We have developed a comprehensive kinematic model for rigid origami of panels with nonzero thickness. This is done by identifying a spatial linkage model that is kinematically equivalent to the rigid origami of a zero-thickness sheet. In other words, the motion of the spatial linkage mimics that of the spherical linkage commonly used to model rigid origami. To achieve this, we identified a spatial linkage that has the angular conditions for arrangement of fold lines identical to that of the spherical linkage and then proved analytically that their motions are precisely alike.

The thick-panel counterparts to four-, five-, and six-crease vertex origami patterns are over-constrained spatial linkages. The number of such linkages is rather limited (17). It is relatively straightforward for four-crease origami patterns because only one spatial 4R linkage exists. However, five- and six-crease single-vertex patterns commonly comprise two or three degrees of freedom, whereas their corresponding spatial overconstrained linkages have only one mobility degree of freedom. In these cases, equivalence can only be accomplished through reducing the degrees of freedom of the former by symmetry or other means. This may be beneficial for practical applications because the folding of thick panels can be more easily controlled owing to their single degree of freedom. Moreover, the synthesis can also be used for origami patterns consisting of a mixture of vertices with various creases. The folding sequence of a thick-panel origami based on a pattern with both four- and six-crease vertices is shown in Fig. 4E and movie S1.

REFERENCES AND NOTES

1. Z. You, *Science* **345**, 623–624 (2014).
2. I. Hagiwara, in *System Simulation and Scientific Computing*, T. Xiao, L. Zhang, S. Ma, Eds. (Springer, Berlin, 2012), pp. 259–268.
3. K. Miura, "Method of packaging and deployment of large membrane in space," 31st Congress of International Astronautical Federation, New York, Paper A 31 (1980), pp. 1–10.
4. S. Felton, M. Tolley, E. Demaine, D. Rus, R. Wood, *Science* **345**, 644–646 (2014).
5. T. Tachi, in *Origami*⁵, P. Wang-Iverson, R. J. Lang, M. Yim, Eds. (AK Peters, Natick, MA, 2011), pp. 253–264.
6. B. J. Edmondson *et al.*, "An offset panel technique for thick rigidly foldable origami," presented in ASME 2014 International Design Engineering Technical Conferences, Buffalo, NY, 17 to 21 August 2014.
7. C. S. Hoberman, U.S. Patent No. 4,780,344 (1988).
8. I. A. N. De Temmerman, M. Mollaert, T. Van Mele, L. De Laet, *Int. J. Space Structures* **22**, 161–168 (2007).
9. J. Phillips, *Freedom of Machinery*, vol. II (Cambridge Univ. Press, Cambridge, 1990).
10. T. Hull, *Congr. Numer.* **100**, 215–224 (1994).
11. C. H. Chiang, *Kinematics of Spherical Mechanisms* (Krieger Publishing, Malabar, FL, 2000).
12. G. T. Bennett, *Engineering* **76**, 777–778 (1903).
13. J. S. Beggs, *Advanced Mechanism* (Macmillan Company, New York, 1966).
14. F. E. Myard, *Soc. Math. France* **59**, 183–210 (1931).
15. R. Bricard, Leçons de cinématique, *Tome II Cinématique Appliquée* (Gauthier-Villars, Paris, 1927), pp. 7–12.
16. S. Randlett, *The Art of Origami: Paper Folding, Traditional and Modern* (Faber and Faber, London, 1963)
17. Z. You, Y. Chen, *Motion Structures* (Spon Press, Oxford, UK, 2012).

STRETCHY ELECTRONICS

Hierarchically buckled sheath-core fibers for superelastic electronics, sensors, and muscles

Z. F. Liu,[1,2,3] S. Fang,[1,3]* F. A. Moura,[1,4] J. N. Ding,[2,10] N. Jiang,[1,3] J. Di,[1] M. Zhang,[5] X. Lepró,[1] D. S. Galvão,[4] C. S. Haines,[1] N. Y. Yuan,[2,3] S. G. Yin,[3,6] D. W. Lee,[3] R. Wang,[2,3] H. Y. Wang,[3,6] W. Lv,[2,3] C. Dong,[2,3] R. C. Zhang,[3,6] M. J. Chen,[2,3] Q. Yin,[2,3] Y. T. Chong,[3] R. Zhang,[7,8] X. Wang,[8] M. D. Lima,[1] R. Ovalle-Robles,[9] D. Qian,[8] H. Lu,[8] R. H. Baughman[1,3]*

Superelastic conducting fibers with improved properties and functionalities are needed for diverse applications. Here we report the fabrication of highly stretchable (up to 1320%) sheath-core conducting fibers created by wrapping carbon nanotube sheets oriented in the fiber direction on stretched rubber fiber cores. The resulting structure exhibited distinct short- and long-period sheath buckling that occurred reversibly out of phase in the axial and belt directions, enabling a resistance change of less than 5% for a 1000% stretch. By including other rubber and carbon nanotube sheath layers, we demonstrated strain sensors generating an 860% capacitance change and electrically powered torsional muscles operating reversibly by a coupled tension-to-torsion actuation mechanism. Using theory, we quantitatively explain the complementary effects of an increase in muscle length and a large positive Poisson's ratio on torsional actuation and electronic properties.

Highly elastic electrical conductors are needed for stretchable electronic circuits, pacemaker leads, light-emitting displays, batteries, supercapacitors, and strain sensors (1). For such purposes, conducting elastomers have been fabricated by incorporating conducting particles in rubber (2–5) or by attaching sheets of conducting nanofibers (6–9), graphene sheets (10, 11), or coiled or serpentine conductors to a rubber sheet or fiber (12–17). Although reversible strains exceeding 500% have been demonstrated, the quality factor (Q, the percent strain divided by the percent resistance change) has been below three for such large strains (17–20). Elastomeric conductors with very low quality factors are useful as strain sensors, but the other applications noted above would benefit from the realization of very high quality factors. The availability of conducting fibers that can be stretched to great extents without

significantly changing conductivity could enable the deployment of superelastic fibers as artificial muscles, electronic interconnects, supercapacitors, or light-emitting elements.

We replaced the frequently used laminate of a carbon nanotube (CNT) sheet wrapped on a stretched rubber sheet with a multilayer CNT sheath wrapped on a rubber fiber core (21, 22). We enabled additional functions by including other rubber and CNT sheath layers. The conducting sheaths were derived from highly oriented multiwalled CNT aerogel sheets, which were drawn from CNT forests (21). Three basic configurations were deployed: NTS_m@fiber, rubber@NTS_m@fiber, and NTS_n@rubber@NTS_m@fiber. NTS_m@fiber denotes m carbon nanotube sheet (NTS) layers deposited on top of a rubber fiber core, rubber@NTS_m@fiber is a rubber-coated NTS_m@fiber, and NTS_n@rubber@NTS_m@fiber indicates an NTS_n sheath (where n is the number of NTS layers) on a rubber@NTS_m@fiber core.

The rubber fiber core was highly stretched (typically to 1400% strain) during the wrapping of NTS layers, and the CNT orientation was parallel to the rubber fiber direction (Fig. 1A). For the preparation of rubber@NTS_m@fibers, the outermost rubber coating was applied while the rubber core was fully stretched, whereas for the preparation of NTS_n@rubber@NTS_m@fibers, the thicker rubber layer used as a dielectric was deposited on an NTS_m@fiber that was not stretched (22). The parallel orientations of CNT fibers and the rubber core, the substantial strain applied during sheath wrapping, and the use of a large m resulted in the observed hierarchical two-dimensional buckling and corresponding

¹Alan G. MacDiarmid NanoTech Institute, University of Texas at Dallas, Richardson, TX 75080, USA. ²Jiangsu Collaborative Innovation Center of Photovoltaic Science and Engineering, Changzhou University, Changzhou 213164, China. ³Jiangnan Graphene Research Institute, Changzhou 213149, China. ⁴Applied Physics Department, State University of Campinas, Campinas, SP 13081-970, Brazil. ⁵High-Performance Materials Institute, Florida State University, Tallahassee, FL 32310, USA. ⁶Institute of Materials Physics, Tianjin University of Technology, Tianjin 300384, China. ⁷School of Astronautics, Northwestern Polytechnical University, Xi'an 710072, China. ⁸Department of Mechanical Engineering, University of Texas at Dallas, Richardson, TX 75080, USA. ⁹Lintec of America, Nano-Science and Technology Center, Richardson, TX 75081, USA. ¹⁰Micro/Nano Science and Technology Center, Jiangsu University, Zhenjiang 212013, China.
*Corresponding author. E-mail: sfang@utdallas.edu (S.F.); ray.baughman@utdallas.edu (R.H.B.)

Origami of thick panels

Yan Chen, Rui Peng, and Zhong You

Expanding origami to thicker materials

A vast array of origami patterns can be applied to the folding of any material of near-zero thickness, such as paper. However, the folding of thick materials requires adding material and offsets. Chen *et al.* develop a general model in which the standard spherical linkages (creases) are replaced with rigid panels connected via offset folds, so that the folding motion of both near-zero–thickness and thick objects is the same. Furthermore, the hinges are constrained to move in only one direction, which is important for applications such as unfolding solar panels in space or large engineering structures, where you want the folding to occur automatically.

Science, this issue p. 396

View the article online
https://www.science.org/doi/10.1126/science.aab2870
Permissions
https://www.science.org/help/reprints-and-permissions